Atmospheric Environment 240 (2020) 117807

Contents lists available at ScienceDirect

Atmospheric Environment

journal homepage: http://www.elsevier.com/locate/atmosenv

# Hourly measurements of organic molecular markers in urban Shanghai, China: Observation of enhanced formation of secondary organic aerosol during particulate matter episodic periods

Xiao He [a], Qiongqiong Wang [b], X.H. Hilda Huang [a], Dan Dan Huang [c], Min Zhou [c], Liping Qiao [c], Shuhui Zhu [b,c], Ying-ge Ma [c], Hong-li Wang [c], Li Li [d], Cheng Huang [c,**], Wen Xu [e], Douglas R. Worsnop [e], Allen H. Goldstein [f,g], Jian Zhen Yu [a,b,*]

[a] Division of Environment & Sustainability, Hong Kong, China
[b] Department of Chemistry, The Hong Kong University of Science & Technology, Clear Water Bay, Hong Kong, China
[c] State Environmental Protection Key Laboratory of the Formation and Prevention of Urban Air Pollution Complex, Shanghai Academy of Environmental Sciences, Shanghai, China
[d] Institute of Environmental Pollution and Health, Shanghai University, Shanghai, 200072, China
[e] Aerodyne Research Inc., Billerica, MA, USA
[f] Department of Environmental Science, Policy, and Management, USA
[g] Department of Civil and Environmental Engineering, University of California, Berkeley, CA, USA

## HIGHLIGHTS

- Online measurement of individual aerosol organics was made for the first time in urban Shanghai.
- Secondary organic aerosol (SOA) tracers specific to a few common precursors were tracked.
- Significant mass enhancement of SOA tracers and nitrate was observed during 5 $PM_{2.5}$ episodes.
- Toluene and other monoaromatics SOA tracer had a mass increment of 5.6 during episodes vs. <2 for primary pollutants.
- The diagnostic ratio of two α-pinene SOA tracers suggested fresh SOA in urban Shanghai.

## GRAPHICAL ABSTRACT

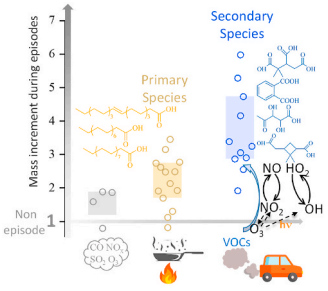


## ARTICLE INFO

*Keywords:*
Online organic compound speciation
SOA formation
Episodes in urban Shanghai
Thermal desorption Aerosol Gas chromatograph (TAG)

## ABSTRACT

Field campaigns rarely measure individual polar organic compounds online, leaving unexplored their potential in tracking the formation dynamics of secondary organic aerosol (SOA). In a three-week-long field campaign in urban Shanghai, we deployed a commercial Thermal desorption Aerosol Gas chromatograph system (TAG) that integrates sampling, in-situ derivatization, and thermal desorption gas chromatography-mass spectrometric analysis, producing hourly measurement of polar organics including a set of biogenic and anthropogenic SOA tracers. The abundance and variations of these SOA tracers were examined in relation to five $PM_{2.5}$ episodes,

* Corresponding author. Department of Chemistry, The Hong Kong University of Science & Technology, Clear Water Bay, Hong Kong, China.
** Corresponding author.
*E-mail addresses:* huangc@saes.sh.cn (C. Huang), jian.yu@ust.hk (J.Z. Yu).

https://doi.org/10.1016/j.atmosenv.2020.117807
Received 13 May 2020; Received in revised form 17 July 2020; Accepted 21 July 2020
Available online 29 July 2020

varying from 4 to 64 h in duration, during the field campaign from 9 November to 3 December 2018. The episodes were associated with stagnant air parcels. In comparison with the non-episodic hours, the episodic hours showed distinct chemical characteristics of a large mass increment of nitrate (an average of 4.7 fold) and secondary organic compounds (~3–6.4 fold), exceeding those of primary pollutants (1.6–1.9 fold). These results clearly indicate the significant contributions of secondary inorganic and organic production processes to forming $PM_{2.5}$ episodes. The SOA concentration estimated by the set of TAG-measured SOA tracers reached an average concentration of 2.6 μg/m$^3$, accounting for a significant portion of OA in view of that the total organic matter (OM) in $PM_1$ measured by an Aerosol Mass Spectrometer was 7.9 μg/m$^3$. Among them the SOA attributed to monoaromatic compounds (e.g., toluene) accounted for a noticeable portion of the total OM, implying that control strategies targeting local anthropogenic emissions would be effective in reducing the severity of episodic PM pollution. Examining the ratio of two monoterpene-derived SOA products, we found evidence of less-aged SOA in urban Shanghai, and this result was collaborated by the O/C value (0.4) of bulk OA. This work demonstrates hourly SOA tracer measurements by TAG are uniquely specific on identification of major SOA precursors for episodic events and observing the evolution of SOA.

## 1. Introduction

Organic matter accounts for a significant fraction of $PM_{2.5}$ mass concentration, normally 20–80%, with varying composition under diverse environmental conditions (Kim et al., 2017; Li et al., 2017; Zhang et al., 2017). Organic aerosol (OA) exposure could cause respiratory and cardiovascular system deterioration and is linked with elevated mortality on a global scale (Lelieveld et al., 2013). Exposure to $PM_{2.5}$ episodes, often with significantly elevated OA concentration, is found to be closely associated with oxidative inflammatory responses (Ho et al., 2016; Huttunen et al., 2012; Pope et al., 2016). OA speciation at a molecular level, particularly the identification and quantification of source-specific tracers, has value in elucidating multiple aerosol sources, clarifying aerosol evolution with respect to atmospheric oxidants, and evaluating the influence of OA on human health.

OA speciation has been traditionally done by collection of filter samples (sampling duration ranging from a few hours to days), followed by laborious sample treatment and instrumental analysis. Such sampling and analysis settings render the OA molecular data to be of low time resolution and ill-suited for capturing the fast fluctuation of meteorological parameters (e.g., temperature, relative humidity (RH), and planetary boundary layer height), pollution emissions (e.g., rush hour vehicle emissions), and atmospheric conditions (e.g., atmospheric oxidants) within the time span of a day cycle (Rastogi et al., 2015; Spira-Cohen et al., 2010; Wang et al., 2015). The development of online instruments in the past decade allowed us to obtain PM composition information with much higher time resolution (e.g., hourly) and has opened up the possibility for new understanding on physical and chemical processes of atmospheric PM such as pollutant transport from sources to receptor sites, chemical transformation of PM components and formation pathways of secondary organic aerosols (SOA) (Jayne et al., 2000; Jimenez et al., 2003; Williams et al., 2006).

Several online instruments with hourly time resolution for major $PM_{2.5}$ components have been commercialized over the past one and a half decades. The Monitor for AeRosols and GAses in ambient air (MARGA) is a fully autonomous sampling and measurement instrument that continuously measures the water-soluble gas and aerosol components. The semi-continuous organic carbon/elemental carbon (OC/EC) instrument provides hourly OC/EC concentrations by a stepped-temperature ramp up to ~850 °C (Saarikoski et al., 2008). The online X-ray fluorescence (XRF) spectrometer determines the concentration of airborne metals on the principle of excitation of the inner electronic shell of the metal with the subsequent X-ray emission induced by the re-occupation of the shell vacancy by an electron from an outer shell (Furger et al., 2017). A recent addition to the online instrumentation family focuses on measuring individual organic compounds, namely the Thermal desorption Aerosol Gas chromatography (TAG), developed by Goldstein and co-workers at UC Berkeley with Hering and Kreisberg at Aerosol Dynamics Inc., and commercialized by Aerodyne Research Inc (Billerica, MA, USA). TAG integrates online aerosol sampling, thermal desorption, and separation and quantification of individual organic compounds by gas chromatography-mass spectrometry (GC/MS) (Williams et al., 2006).

An additional online instrument that is particularly relevant to OA characterization is the aerosol mass spectrometer (AMS) developed by Aerodyne Research Inc. AMS outputs mass concentrations of non-refractory PM compositions in bulk by monitoring ion fragments that are attributable to sulfate, nitrate, ammonium, chloride, and organics (Canagaratna et al., 2007; Li et al., 2017). AMS has been widely used in obtaining real-time chemical composition of PM, including bulk OA. We note that AMS data is less uniquely linked to aerosol sources than the molecular or elemental tracers, as the molecular information is partially lost in the process of forming fragment ions in AMS.

In this work, an array of online instruments was deployed in a field campaign in Shanghai, China. For the first time in this region, OA speciation of hourly resolution was achieved through deploying a TAG. The continuous measurement of individual organic molecules enables probing sources of primary OA and formation of SOA via their characteristic molecular markers. The examination of primary OA tracers from this field campaign is reported in Wang et al, (2020). In this work, the focus is on a set of polar organic compounds, including biogenic and anthropogenic SOA tracers, with the aim to advance the understanding of the SOA formation during high $PM_{2.5}$ episodic events. The findings reveal a significantly enhanced contribution by anthropogenic SOA to the five $PM_{2.5}$ episodic events encountered in the campaign, providing measurement-based evidence in help prioritizing control strategies for future air quality improvement. Source apportioning using the combined primary OA and SOA tracer data in this work is described in Li et al. (2020).

## 2. Experiment

### 2.1. Site description and sampling

The campaign was conducted at a monitoring station on the site of Shanghai Academy of Environmental Sciences (SAES) (31.17°N, 121.43°E) in the southwest of urban Shanghai (see map location in Fig. S1 in supporting information (SI)). SAES is located in a commercial and residential district, with a main road for vehicular traffic ~100 m away. The campaign period with TAG monitoring data coverage was from 9 November to 3 December 2018. Air masses impacting the sampling site were examined and categorized into 4 groups (Fig. S3). More details will be described in section 3.2.

### 2.2. Quantification of individual organic compounds in PM by the TAG system

The TAG system was placed on the eighth floor at the site, ~25 m above the ground. It was operated on a 2-h basis for each sampling and analysis cycle. The $PM_{2.5}$ sampling started at each odd hour at a flow

rate of 8 LPM and lasted for 1 h, coinciding with the duration spent on the GC-MS analysis step (Fig. S5). Field blank samples were collected once every 2 day at a fixed time (1:00–3:00 a.m.). A total of 270 valid samples and 11 blank samples were collected throughout the campaign.

The schematic diagram of the TAG deployed in this work is shown in Fig. S4. A detailed description of the working principle of TAG can be found in previous publications (Isaacman et al., 2014; Williams et al., 2006). In brief, ambient air is drawn into the system through the sampling inlet, with RH of the inlet regulated by a Nafion dryer (PERMA PURE, MD-700-24S-3). A carbon denuder (model: ADI-DEN2) is placed downstream from the drier to remove volatile and semi-volatile vapor phase organics with minimal particle loss (<5%) (Zhao et al., 2013). The particles in the air stream are deposited into a 9-jet impactor collection and thermal desorption (CTD) cell maintained at room temperature during sampling (Fig. S4a). At the end of the sampling, 5 μL of internal standard (IS) mixture (Table S1) is spiked into the CTD cell through a 6-port automatic valve (Fig. S4b). At the stage of thermal desorption (Fig. S4c), a helium stream saturated with the derivatization agent N-methyl-N-(trimethylsilyl)trifluoroacetamide (MSTFA) flows through the CTD cell. The cell is heated from room temperature to 330 °C in 6 min and kept at this temperature for 14 min. The thermally desorbed organic species are condensed onto the focusing trap (FT), with the FT cooled by a fan. At the end of the derivatization step, the CTD cell is purged with pure He to vent the excess MSTFA. FT is then heated to 315 °C in 12 min and the helium flow carries the target compounds into the GC column head followed by GC/MS analysis. Fig. S5 shows the temperature programs of CTD, FT and "to-GC-arm" in one sampling/analysis cycle. A detailed description of helium flow is given in Text S2 in the SI.

A DB-5MS column (30 m × 0.25 mm × 0.25 μm, J&W Scientific) is used in the GC-MS analysis (He et al., 2018). The GC temperature program starts at an initial temperature of 45 °C, ramps up to 200 °C at a rate of 35 °C/min, held for 2 min, and further increases to 300 °C at 10 °C/min. The MS analysis is conducted in electron ionization positive (EI+) mode over an *m/z* range of 50–650. The ion source, quadrupole, and interface temperatures are kept at 230, 150, and 280 °C, respectively. Table 1 lists the target polar organic compounds discussed in this work. The preparation of working external standards and ISs and data quality assessment are provided in the SI (Text S2 and S3).

### 2.3. Other measurements

An array of online instruments was deployed at the site and the details of these instruments, except for TAG and AMS, were provided in previous publications (Qiao et al., 2014; Wang et al., 2018). Briefly, the $PM_{2.5}$ mass concentration was measured by a beta attenuation particulate monitor (Thermo Fisher Scientific, FH 62 C14 series); major water-soluble ionic species ($NO_3^-$, $Cl^-$, $SO_4^{2-}$, $Na^+$, $NH_4^+$, $K^+$, $Mg^{2+}$, and

**Table 1**
Statistical summary of concentrations of polar organic compounds measured by TAG and the major species in $PM_{2.5}$ during episodes and non-episode periods during the field campaign.

| | Compound | Episodes | | Non-episodes | | Increment ratio[a] | Internal standard |
|---|---|---|---|---|---|---|---|
| | | Avg | Std | Avg | Std | | |
| Polar organic species (ng/m$^3$) | | | | | | | |
| Dicarboxylic acids | Succinic acid | 87.86 | 42.91 | 26.18 | 25.16 | **3.36** | Succinic acid-$d_4$ |
| | Glutaric acid | 48.54 | 29.67 | 9.57 | 12.19 | **5.07** | |
| | Adipic acid | 37.25 | 17.44 | 8.30 | 7.49 | **4.49** | Azelaic acid-$d_{14}$ |
| | Pimelic acid | 1.55 | 0.67 | 0.49 | 0.36 | **3.16** | |
| | Suberic acid | 4.43 | 1.92 | 1.56 | 1.30 | 2.84 | |
| | Azelaic acid | 10.40 | 4.54 | 4.75 | 3.85 | 2.19 | |
| Hydroxyl-carboxylic acids | Citramalic acid | 58.53 | 36.12 | 15.42 | 18.36 | **3.80** | |
| | Tartaric acid | 107.71 | 62.77 | 16.96 | 21.20 | **6.35** | Citric acid-$d_4$ |
| | Glyceric acid | 96.84 | 43.50 | 32.99 | 35.51 | 2.94 | Succinic acid-$d_4$ |
| Aromatic acids | 3-hydroxybenzoic acid | 0.85 | 0.39 | 0.35 | 0.24 | 2.43 | Phthalic acid-3,4,5,6-$d_4$ |
| | 4-hydroxybenzoic acid | 1.12 | 0.53 | 0.46 | 0.38 | 2.43 | |
| | Isophthalic acid | 0.90 | 0.40 | 0.35 | 0.22 | 2.57 | |
| | 1,2,3-BTCA[b] | 0.80 | 0.53 | 1.06 | 0.92 | 0.75 | |
| | 1,2,4- BTCA | 0.86 | 0.53 | 0.77 | 0.74 | 1.12 | |
| | 1,3,5- BTCA | 0.10 | 0.09 | 0.08 | 0.09 | 1.25 | |
| | Terephthalic acid | 10.22 | 4.68 | 3.75 | 3.38 | 2.73 | |
| Fatty acids | Palmitic acid | 76.24 | 39.18 | 41.30 | 35.90 | 1.85 | Palmitic acid-$d_{31}$ |
| | Stearic acid | 38.24 | 18.59 | 20.55 | 15.28 | 1.86 | Stearic acid-$d_{35}$ |
| | Oleic acid | 10.45 | 6.32 | 5.04 | 5.85 | 2.07 | |
| Cholesterol | Cholesterol | 7.35 | 3.08 | 6.00 | 2.29 | **1.23** | Cholesterol-2,2,3,4,4,6-$d_6$ |
| Saccharides | Galactosan | 2.49 | 1.15 | 0.73 | 0.83 | **3.41** | Levoglucosan-$d_7$ |
| | Mannosan | 3.21 | 1.48 | 1.03 | 1.07 | **3.12** | |
| | Levoglucosan | 88.93 | 39.79 | 32.98 | 29.96 | 2.70 | |
| | Mannitol | 3.49 | 1.53 | 3.35 | 2.26 | 1.04 | Glucose-$d_7$ |
| | Glucose | 12.34 | 5.63 | 7.58 | 5.15 | 1.63 | |
| | Sucrose | 41.80 | 21.44 | 57.36 | 54.26 | 0.73 | |
| α-pinene SOA tracers | Pinic acid | 34.91 | 14.85 | 10.91 | 10.02 | **3.20** | Azelaic acid-$d_{14}$ |
| | 3-MBTCA[c] | 11.24 | 5.20 | 3.04 | 4.08 | **3.70** | |
| Toluene and other monoaromatics SOA tracer | DHOPA[d] | 10.66 | 4.84 | 1.89 | 2.56 | **5.64** | |
| Naphthalene SOA tracer | Phthalic acid | 20.06 | 10.50 | 5.65 | 4.04 | **3.55** | Phthalic acid −3,4,5,6-$d_4$ |
| Major species (μg/m$^3$) | | | | | | | |
| $PM_{2.5}$ | | 100.78 | 42.88 | 31.80 | 19.61 | **3.17** | |
| $NO_3^-$ | | 33.96 | 14.31 | 7.17 | 5.72 | **4.74** | |
| $NH_4^+$ | | 14.29 | 6.11 | 3.84 | 2.62 | **3.72** | |
| $SO_4^{2-}$ | | 11.03 | 4.64 | 4.96 | 2.71 | 2.22 | |
| $PM_1$ OM | | 27.14 | 12.13 | 10.00 | 7.37 | 2.71 | |

[a] Mass increasement ratio larger than **3** is highlighted in bold.
[b] BTCA: benzene-tricarboxylic acid.
[c] 3-MBTCA: 3-methyl-1,2,3-butanetricarboxylic acid.
[d] DHOPA: 2,3-dihydroxy-4-oxopentanoic acid.

$Ca^{2+}$) in $PM_{2.5}$ were measured by MARGA (ADI, 2080; Applikon Analytical B.V.); elements in $PM_{2.5}$ (Al, P, Cl, K, Ca, Sc, V, Cr, Mn, Fe, Co, Ni, Cu, Zn, Ga, Ge, As, Se, Br, Sr, Nb, Mo, Sn, Pd, Ag, Cd, In, Sb, Sn, Sb, Ba, Pt, Au, Hg, Ti, Pb, and Bi) were monitored by an online XRF spectrometer (Xact® 625, Cooper Environmental Services, Tigard, OR, USA); black carbon (BC) was measured by an Aethalometer (Magee Scientific Company, Berkeley, CA, USA). Organic matter (OM) in $PM_1$ was obtained by an Aerodyne high-resolution time-of-flight Aerosol Mass Spectrometer (HR-ToF-AMS). These instruments were located on the rooftop of an eight-floor building at the site. All the above-mentioned online instruments output 1-h resolution data, and the data at odd hours is compiled to compare with the TAG data.

Criteria gaseous pollutants including $SO_2$, $O_3$, $NO_2$, NO, and CO together with meteorological parameters including temperature, RH, atmosphere pressure, visibility, wind speed (WS), and wind direction (WD) were also recorded. The time series of wind speed and RH are shown in Fig. 1a. Temperature is ruled out as an influential parameter on PM episodic event. Its temporal radiation is shouwn in Fig. S6, together with the time series of $PM_{2.5}$ concentration.

## 3. Results and discussion

### 3.1. Characteristics of $PM_{2.5}$ mass and the major components

Hourly $PM_{2.5}$ mass concentration ranged from 8 to 154 μg/m$^3$ and had a campaign-average of 47.4 ± 33.6 μg/m$^3$. A $PM_{2.5}$ mass closure is conducted by inputting the hourly major constituent data into the following equation:

Reconstructed $PM_{2.5}$ mass = crustal material (2.2[Al] + 2.49[Si] + 1.63[Ca] + 2.42[Fe] + 1.94[Ti])

+ BC + OM

+ sulfate + nitrate + ammonium

+ other water-soluble ions (sum of $Cl^-$, $Na^+$, $K^+$, $Mg^{2+}$, and $Ca^{2+}$)

+ trace elements

OM is approximated to be $PM_1$ OM by AMS, providing a lower estimate of the actual $PM_{2.5}$ OM. Trace elements are the sum of P, Sc, V, Cr, Mn, Co, Ni, Cu, Zn, Ga, Ge, As, Se, Br, Sr, Nb, Mo, Sn, Pd, Ag, Cd, In, Sb, Sn, Sb, Ba, Pt, Au, Hg, Pb, and Bi. The hourly measured and reconstructed $PM_{2.5}$ masses are highly correlated (R = 0.97) and in good agreement (slope = 0.97), as seen in their time-series plots (Fig. 1c). The three secondary inorganic ions, i.e., nitrate (12.9 ± 12.8 μg/m$^3$), sulfate (6.3 ± 3.3 μg/m$^3$) and ammonium (6.2 ± 5.1 μg/m$^3$), comprised of approximately half (54%) of the total $PM_{2.5}$ mass. OM had an average concentration of 14.1 ± 11.1 μg/m$^3$, accounting for ~30%. Crustal material and BC were less abundant constituents, taking up 6% and 5% of the $PM_{2.5}$ mass, respectively.

### 3.2. Determination of PM episodic periods

PM episodic periods were identified based on hourly air quality index (AQI). In this work, we define episodic hours to be those periods with AQI exceeding 100. The overall AQI considers six atmospheric pollutants ($SO_2$, $NO_2$, CO, $O_3$, $PM_{10}$, and $PM_{2.5}$) and is the maximum of the six individual AQIs (IAQIs). The computation of individual AQIs from monitoring concentrations is detailed in Text S4 in SI. Fig. 1b shows the time series of color coded IAQIs. Clearly, $PM_{2.5}$ was invariably the determinant pollutant for the overall AQI. A total of five episodic periods emerged, lasting from 4 to 64 h. Table 2 lists the starting and ending time, the average $PM_{2.5}$, wind speed (WS), and RH in each episode. Among the five episodes, four were moderately polluted with

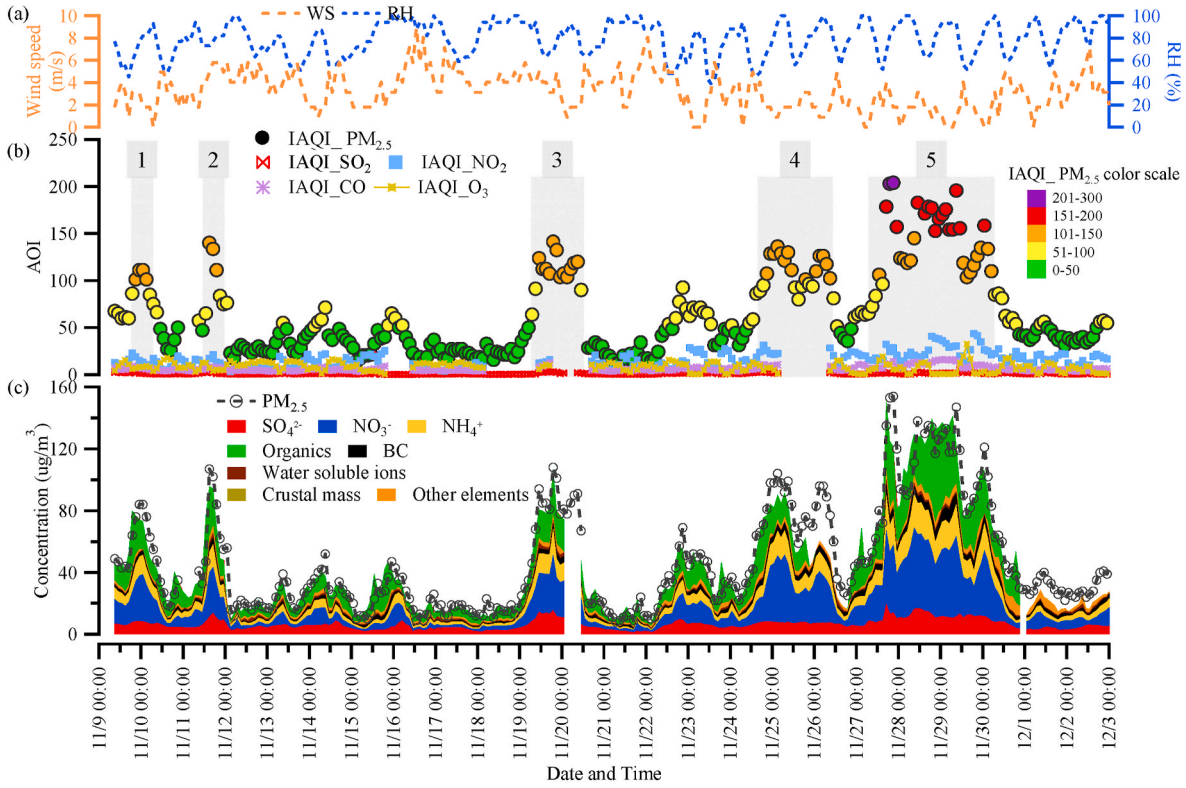


**Fig. 1.** (a) Time series of meteorological conditions; (b) Time series of color-coded AQI, and IAQI for $PM_{2.5}$, $SO_2$, $NO_2$, CO, and $O_3$; (c) Time series of $PM_{2.5}$ and its major components in the campaign period. Water soluble ions are the sum of $Cl^-$, $Na^+$, $K^+$, $Mg^{2+}$, and $Ca^{2+}$. See Eq (1) for the calculation of crustal mass and other elements. The five episodes are shaded in gray in (b); the color scale for AQI is in accordance with Technical Regulation of Ambient Air Quality Index HJ633-2012. (For interpretation of the references to color in this figure legend, the reader is referred to the Web version of this article.)

an AQI of 100–150 and one (E5) was heavily polluted with AQI exceeding 200 in some hours (Fig. 1b).

We next examine the air mass origins under episodic and non-episodic conditions through back-trajectory analysis using the HYSPLIT PC-base model (Hybrid Single-Particle Lagrangian Integrated Trajectory) (Stein et al., 2015). The back-trajectory analysis was run at an elevation of 200 m above ground level and for 48 h. The trajectories were then clustered using an Igor-based software, Zefir (Petit et al., 2017) to classify the air mass origins. The four-cluster solution was determined to be optimal (Fig. S2), consisting of 10% Cluster 1 (C1) from western and northwestern inland China, 25% Cluster 2 (C2) traveling over the ocean to the east, 34% Cluster 3 (C3) circulating over the local areas, and 30% Cluster 4 (C4) from the north and mainly over the ocean with a small part over the continent. The cluster-average chemical composition and $PM_{2.5}$ mass concentration are shown in Fig. S3. It is clear that the air masses originating from inland (C1) and local areas (C3) were associated with higher $PM_{2.5}$ levels (60.3 and 70.3 μg/m$^3$) than air masses from marine sources (C2 and C4, 36.1 and 28.1 μg/m$^3$).

Fig. 2 shows back trajectories associated with individual episodes, along with the major chemical composition of $PM_{2.5}$ during the five episodes and non-episode hours. The air pollution from inland China to the west (C1) influenced the build-up of pollution episodes E1 and E3 while E2, E4, and E5 were mainly under the influence of local air masses (i.e., C3). We note that the two longest episodes (E4 and E5) occurred under stagnant conditions, with the wind speed under 1.8 m/s. The wind speed in E1 and E3 was also lower than the non-episodic hours. In general, an inverse correlation between $PM_{2.5}$ mass concentration and wind speed was observed throughout the campaign (Fig. 1a and c). One exception was E2 (the shortest duration episode), during which an average high wind speed (5.3 m/s) was recorded, and the favorable meteorological conditions may have helped dissipation of PM pollution in a short period of time.

Comparing the percent composition between the episodic and non-episodic hours, a distinct feature is that nitrate was a much more prominent component during episodes (30–41%) than the non-episodic hours (22%), indicating the importance of $NO_x$ emissions in contributing to episodes. The more prominent gain in nitrate has also led to the lower percentage contributions by sulfate and OM, despite that both of their mass concentrations also notably increased during the episodes.

Among episodes, the $PM_{2.5}$ major composition in percentage remain similar except that the OM percentage contribution in E5 (29%) was noticeably higher than the other episodes (21–27%) (Fig. 2a). The OM mass concentration in E5 (33.7 μg/m$^3$) was also significantly higher than in other periods (15.4–24.4 μg/m$^3$) (Fig. 2b).

### 3.3. $PM_{2.5}$ polar organic compounds

We examined here a total of 30 polar organic compounds quantified by TAG, including dicarboxylic acids, hydroxyl-carboxylic acids, aromatic acids, fatty acids, saccharides, and a few SOA tracers. Abbreviations for compound names, if used, are defined in Table 1. Their concentration ranges, as shown in Table 1 and Fig. 3, span three orders of magnitude from 0.05 to ~100 ng/m$^3$ 1,3,5-BTCA is the least abundant (~0.08 ng/m$^3$) while succinic acid, glyceric acid, tartaric acid, palmitic acid, levoglucosan, and sucrose are among the more abundant, exceeding 30 ng/m$^3$ in term of their campaign-average concentrations.

#### 3.3.1. Dicarboxylic acids

Concentrations of dicarboxylic acids ranged from a few to tens of ng/m$^3$. Succinic acid was the most abundant dicarboxylic acid with the average concentration reaching 40.6 ± 42.5 ng/m$^3$ followed by glutaric acid and adipic acid. The potential sources for the homologous series of dicarboxylic acids include primary emissions from vehicle exhausts, photochemical oxidation of anthropogenic emissions such as fossil fuel combustion and industry emissions, and the heterogeneous reactions on the pre-existing particles (Hyder et al., 2012; Mochida et al., 2003; Narukawa et al., 2003).

#### 3.3.2. Hydroxy carboxylic acids

High abundance was observed of the three hydroxy-carboxylic acids during the whole campaign, with the average concentrations for glyceric acid, tartaric acid, and citramalic acid at 47.9 ± 46.0, 38.2 ± 46.5, and 25.4 ± 37.6 ng/m$^3$, respectively.

#### 3.3.3. Aromatic acids

A total of eight aromatic acids were quantified (Table 1) and one of them was phthalic acid and it is described later as part of SOA tracers. Terephthalic acid, a tracer for plastic burning (Simoneit et al., 2005), was the most abundant, with the highest concentration at 10.2 ng/m$^3$ occurring during E5. Its concentration exceeded the sum of the other aromatic acids. This result is consistent with previous offline analysis, which also found the concentration of terephthalic acid was much higher than other aromatic acids at multiple locations (Fu et al., 2010; Li et al., 2015). 3- and 4-Hydroxybenzoic acid (3- and 4-OHBA), products of lignin pyrolysis (He et al., 2018), exhibit excellent correlations with levoglucosan, mannosan and galactosan ($R^2$ = 0.69–0.90), confirming common biomass burning origin. Vanillic acid and syringic acid were detected, however, high background levels was recorded for these two compounds, rendering their quantification not reliable and therefore excluded from our discussion.

#### 3.3.4. Fatty acids

Three fatty acids, mainly related to cooking emissions in urban areas, were measured and their concentrations varied from 1.1 ± 1.2 to 52.9 ± 49.4 ng/m$^3$ (Fig. 3). Such levels were comparable to those reported in other urban areas such as Guangzhou in the Pearl River Delta region (Zhao et al., 2014). Cholesterol, another compound mainly attributable to cooking activities in urban atmospheres, was also detected and had an average concentration of 6.3 ± 1.6 ng/m$^3$.

#### 3.3.5. Sugar compounds

A total of six sugar compounds were quantified in this study and their average concentrations ranged from 1.1 ± 1.2 to 52.9 ± 49.4 ng/m$^3$. As ubiquitous PM constituents, saccharides account for a significant portion of organic aerosols from a global perspective, among which levoglucosan and sucrose were undisputedly the most abundant. During the campaign, the concentration of levoglucosan was 45.9 ± 39.2 ng/m$^3$ (1.0–238 ng/m$^3$), whilst its two isomers, galactosan (1.1 ± 1.2 ng/m$^3$) and mannosan (1.5 ± 1.5 ng/m$^3$) were less than 5% the concentration of levoglucosan. The sugar alcohol, mannitol, reported as a unique tracer

**Table 2**
Synopsis of information about individual episodes and the non-episode periods.

| Episode | Start time | End time | Duration (h) | $PM_{2.5}$ (μg/m$^3$) | Wind speed (m/s) | RH (%) | Temperature (°C) | Cluster[a] |
|---|---|---|---|---|---|---|---|---|
| E1 | 11/9 21:00 | 11/10 3:00 | 6 | 80.0 | 2.46 | 77 | 12.8 | C1 |
| E2 | 11/11 15:00 | 11/11 19:00 | 4 | 97.7 | 5.51 | 77 | 18.0 | C3 |
| E3 | 11/19 11:00 | 11/20 9:00 | 22 | 88.1 | 2.94 | 79 | 11.6 | C1 |
| E4 | 11/24 21:00 | 11/26 9:00 | 36 | 84.8 | 1.76 | 87 | 12.8 | C3 |
| E5 | 11/27 13:00 | 11/30 5:00 | 64 | 111.9 | 1.57 | 81 | 13.6 | C3 |
| Non-episode | | | | 31.8 ± 19.6 | 3.53 | 79 | 15.0 | |

[a] The dominating air mass cluster during each episode is shown in Fig. 2. The clustering of back trajectories is described in Figs. S2 and S3 in the SI.

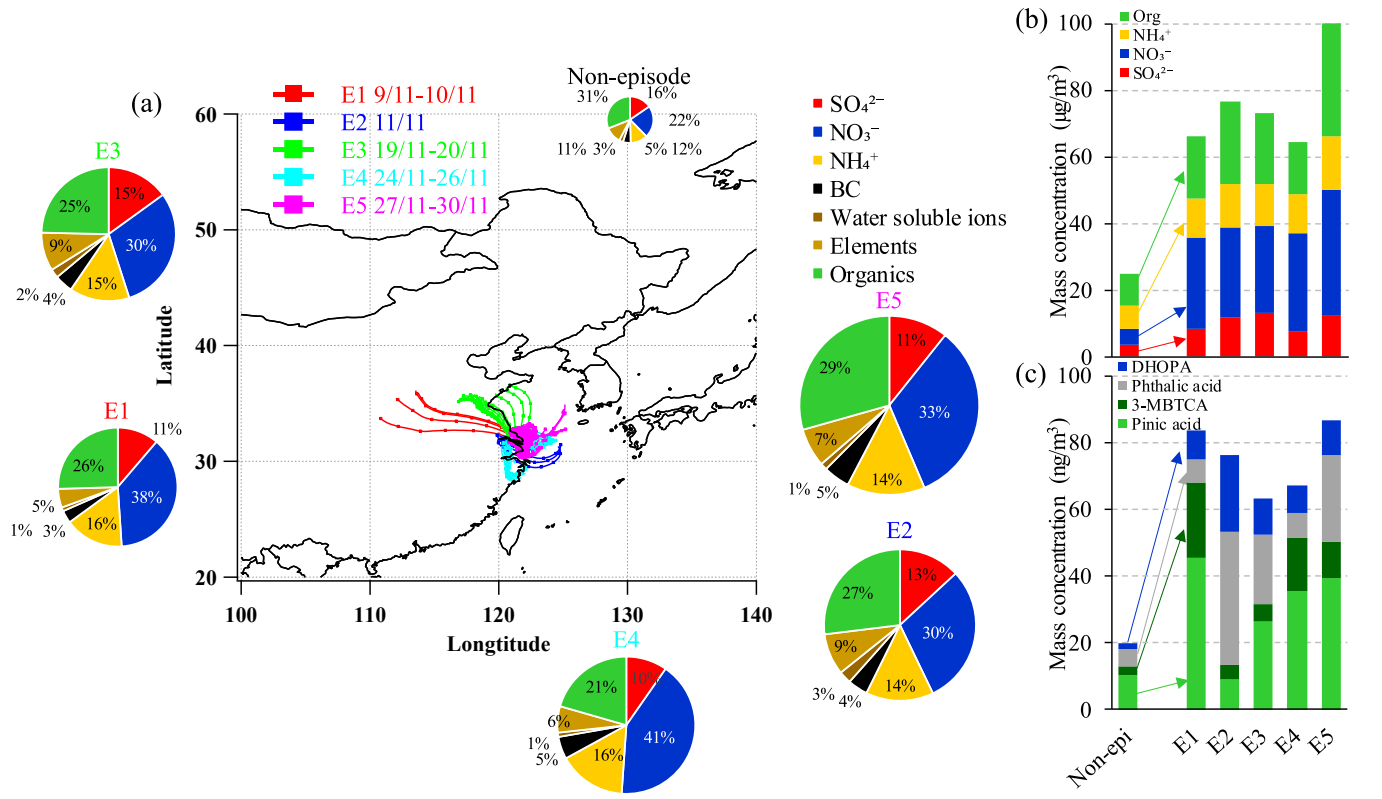


**Fig. 2.** (a) The chemical constituents of $PM_{2.5}$ and the back trajectories of air masses arriving at SAES at an elevation of 200 m during the five episodic events. 48-hour back trajectory was conducted, and a new trajectory started every 2-hr. Back trajectories assigned to different episodes are color coded as shown in the figure. The squares along each trajectory indicate the endpoints of the air parcel every 6-hr; (b) Stack plot of mass concentrations of major $PM_{2.5}$ species; (c) Stack plot of mass concentrations of SOA tracers measured by TAG. (For interpretation of the references to color in this figure legend, the reader is referred to the Web version of this article.)

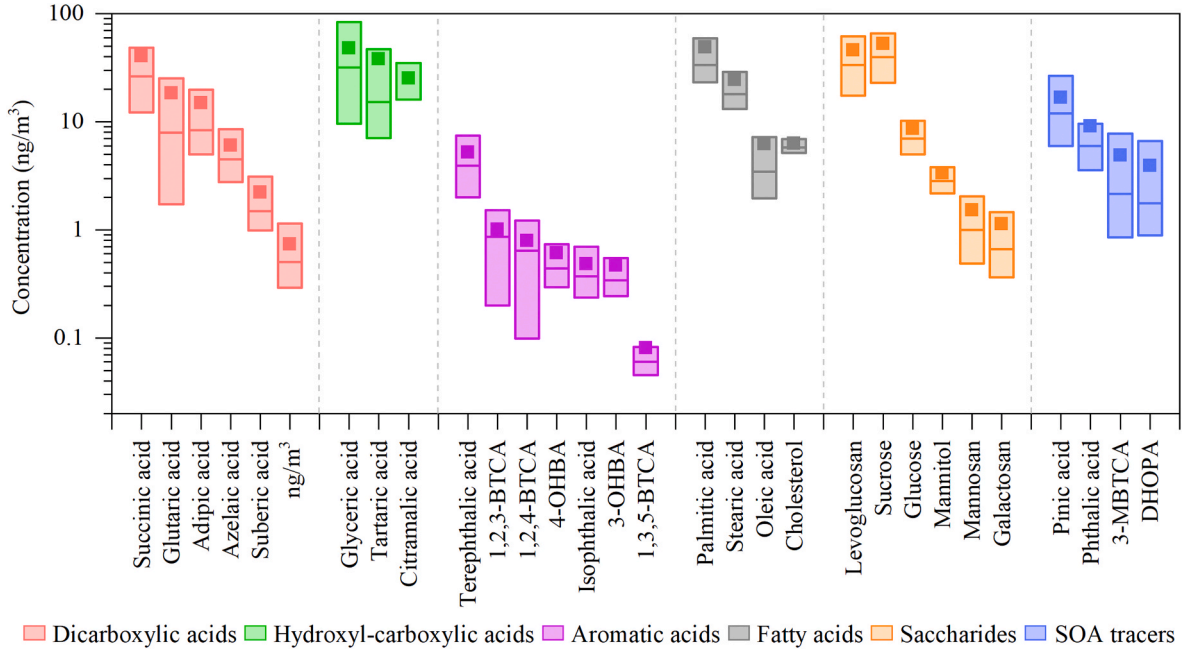


**Fig. 3.** Concentration ranges of the polar organic species measured by the TAG system (BTCA: benzenetricarboxylic acid, OHBA: hydroxybenzoic acid, 3-MBTCA: 3-methyl-1,2,3-butanetricarboxylic acid, DHOPA: 2,3-dihydroxy-4-oxopentanoic acid). The square dot and the horizontal line in the box denote the average and median, respectively. Lower and upper boundaries of the box denote the 25th and 75th percentile of the values.

for the primary biological aerosols from fungal spores, had an average of 3.4 ± 1.9 ng/m$^3$. Sucrose, a disaccharide and emitted predominantly by pollen, averaged at 52.9 ± 49.4 ng/m$^3$ (Bauer et al., 2008; Ho et al., 2014).

### 3.3.6. SOA tracers

We examined the presence of a suite of SOA tracers derived from the following VOC precursors: isoprene, α-pinene, β-caryophyllene, toluene, and naphthalene, which have been reported in our previous filter-based off-line samples in the Pearl River Delta (Hu et al., 2008; Wang et al., 2017). The SOA tracers specific to isoprene precursor were not detected during the campaign period due to the very low isoprene concentration of 0.03 ± 0.02 ppbv (0.004–0.1 ppbv) (unpublished data from collocated online GC/MS measurement). Nor was the SOA tracer specific to β-caryophyllene detected. Two α-pinene SOA tracers, namely pinic acid and 3-methyl-1,2,3-butanetricarboxylic acid (3-MBTCA) were consistently detected. The SOA tracer derived from toluene and other monoaromatics (i.e, 2,3-dihydroxy-4-oxopentanoic acid: DHOPA), and naphthalene SOA tracer (i.e., phthalic acid) were also regularly detected during the whole campaign. The SOA tracers, as for their campaign-average concentration, were comparable to those previously reported for other urban sites (e.g., Beijing and Cleveland). For example, 3-MBTCA concentration is 4.9 ± 5.7 ng/m$^3$ during this campaign, comparing with that of 4.6 ng/m$^3$ measured on Peking University campus in Beijing, China (Guo et al., 2012). DHOPA concentration is 3.9 ± 4.9 ng/m$^3$, comparing with that of 13.3 ng/m$^3$ in urban Beijing, China and 5.1–16.1 ng/m$^3$ at industry sites in Cleveland, USA (Stone et al., 2009).

The time-series of the four SOA tracer compounds are presented in Fig. 4, showing sharp increases of the SOA tracers during episodes. A detailed comparison between episodic and non-episodic periods is given in the next section.

## 3.4. Enhancement of secondary formation during episodes

To indicate and compare the degree of enhancement of different PM components during episodes, we calculated the mass increment ratio (MIR) for individual compounds, i.e., the ratio of the average concentration during the episodic hours over that during the non-episodic hours. The average individual MIR values are listed in Table 1. Fig. 5 shows both the average and range of MIR values, also including those for the inorganic criteria pollutants (i.e., CO, $NO_x$, $SO_2$, and $O_3$) and the four major species of PM (i.e., $NO_3^-$, $NH_4^+$, $SO_4^{2-}$, and bulk organics). A MIR close to 1 indicates no obvious increment. The primary gas pollutants had a MIR of 1.9 for CO and $NO_x$, and 1.6 for $SO_2$, reflecting the concentrating effect associated with the shallower mixing volume during episodes. $NO_3^-$ has the highest ratio (4.7) amongst the major species of $PM_{2.5}$, clearly indicating a significant enhancement in its formation during episodic conditions. $NH_4^+$ has a relatively high MIR (3.7), an expected result of concurrent increase from its close association with nitrate. In comparison, $SO_4^{2-}$ has a lower MIR (2.2), indicating a lesser role for $SO_4^{2-}$ in leading up to the high episodic $PM_{2.5}$.

Bulk organics had a MIR of 2.7, exceeding that of sulfate but lower than that of nitrate. The MIR for the bulk organics lied between primary and secondary organic compounds. For organic compounds of primary origin (e.g., fatty acids, cholesterol, and saccharides), the individual MIR values were mostly in the range of 0.7–2.7, close to that of CO (1.9) (Fig. 5). Two less abundant isomers of levoglucosan (i.e., galactosan and mannosan) had a MIR of 3.4 and 3.1, higher than levoglucosan (2.7) and other primary species. The elevated average MIR values for these biomass burning tracers were mainly caused by their significantly higher concentrations during E3, which was under the influence of long-range transport of air mass from the west (Cluster 1). In comparison, most of the secondary organic compounds (e.g., dicarboxylic acids and SOA tracers) experienced a significant mass increment with MIRs exceeding 3, noticeably higher than those primary organic compounds unassociated with the biomass burning source. DHOPA, the SOA tracer for toluene and other monoaroomatics, had one of the most notable mass increments during the five episodes, with its average MIR at 5.6 and in the range of 4.6–12.0.

It is notable that the two α-pinene derived SOA tracers had a MIR of 3.2 for pinic acid and 3.7 for 3-MBTCA, suggesting the overall oxidation drivers were enhanced during episodic conditions. We also make correlation scatter plots of pinic acid with various known secondary products in Fig. 6, including sulfate, nitrate, the other three SOA tracers, and a dicarboxylic acid (pimelic acid). The Pearson correlation coefficient

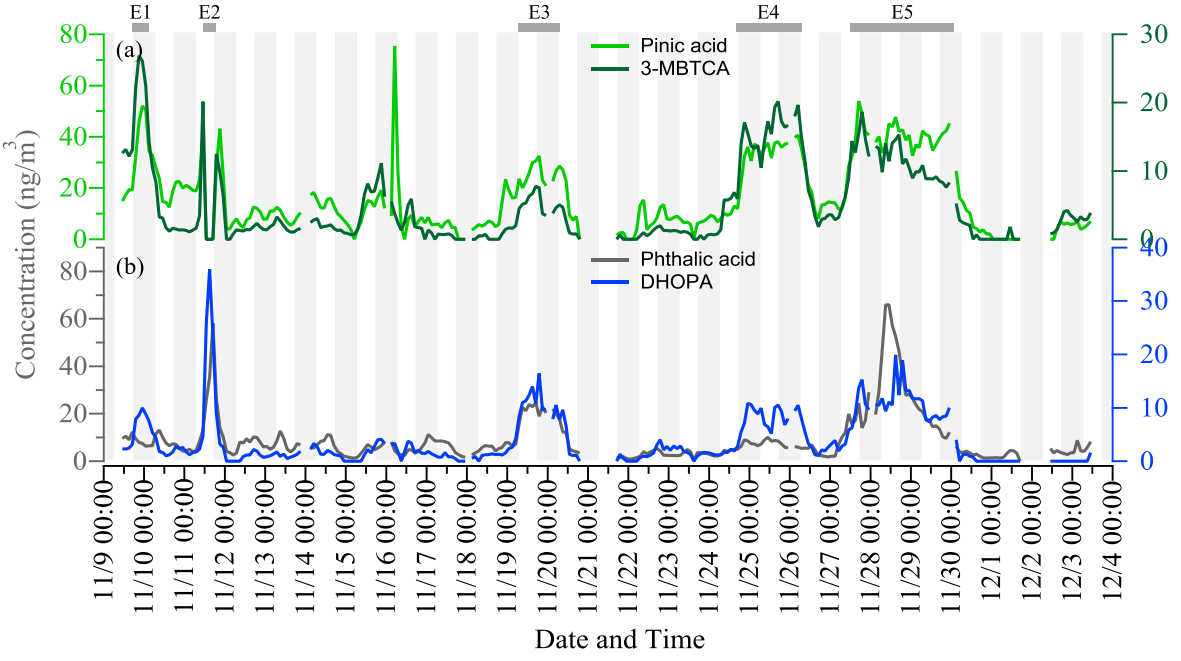


**Fig. 4.** Time series of two α-pinene SOA tracers (pinic acid and 3-MBTCA), one SOA tracer for toluene and other monoaromatics (DHOPA), and one naphthalene SOA tracer (phthalic acid). The five episodes periods are labeled on the top. The shaded and unshaded periods represent nighttime and daytime, respectively.

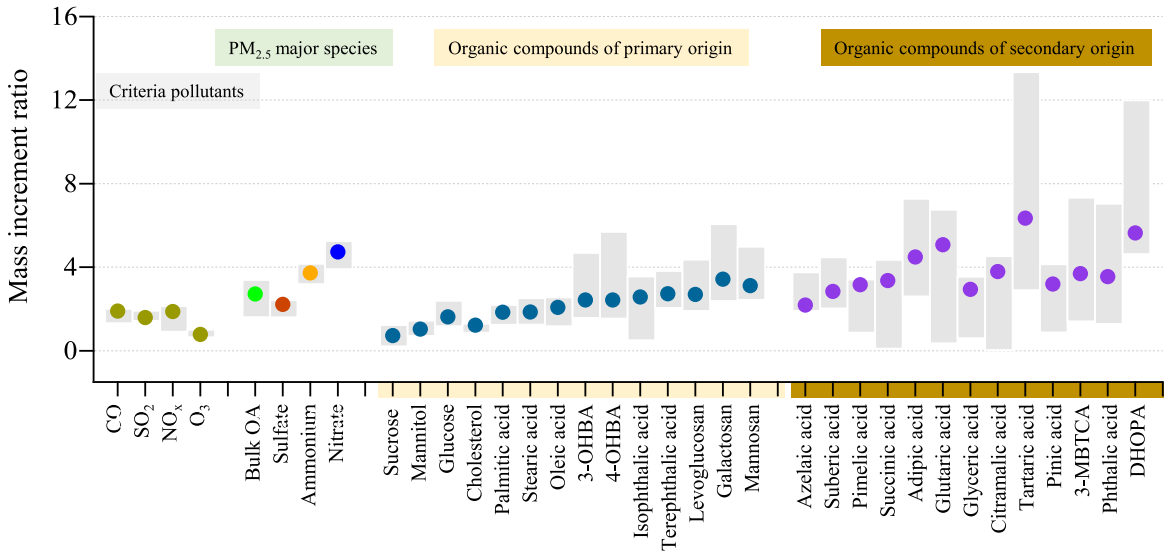


**Fig. 5.** Comparison of the mass increment ratios of episodes-to-non-episodes among different species measured by TAG system. Individual organic compounds are separated into two segments, with the primary OA species shaded in light yellow and the secondary OA species shaded in darker yellow. Middle dots represent the average mass increment ratio and the light gray shades represent the ranges among the five episodes. (For interpretation of the references to color in this figure legend, the reader is referred to the Web version of this article.)

(R) ranges from 0.52 (with phthalic acid) to 0.82 (3-MBTCA and pimelic acid), all exceeding that between pinic acid and BC (R = 0.45), a known major PM component of exclusive primary origin.

Three inferences can be made from Figs. 5 and 6. First and the most important of all, it is unambiguous that secondary OA formation under episodic conditions was enhanced more than what was attributable to compression in mixing volume. Second, the combined effect of atmospheric oxidants was the most plausible driving factor for the positive correlations observed, as the precursors of these secondary products are hugely diverged in both sources and chemical nature. For example, $NO_x$ related to vehicular emissions is the precursor for nitrate in urban environments while α-pinene, a biogenic VOC, is the precursor for pinic acid. Third, comparing the relative position of data point distributions from different episodes reveals differences among the secondary products. For example, for 3-MBTCA, E1 data points are positioned above other episodes (Fig. 6c); for DHOPA, E1 data points fall below half of the E5 data points (Fig. 6d). Such distinct features likely signal divergent pathways from precursor to product and could be potentially explored to gain mechanistic insights.

The third point mentioned above could also be observed when we compare the pair of plots of (DHOPA vs. pinic acid) and (phthalic vs pinic acid) (Fig. 6d and e). A closer examination of the diurnal variation of DHOPA and phthalic acid during E4 and E5, lasting a combined duration of 6 diurnal cycles, shows that these two tracers do not vary in sync (Fig. 7a). Phthalic acid tended to peak during the day and its concentration decreased during nighttime. DHOPA stayed at relatively higher concentrations in the nighttime while its concentration showed a dip during the day. The out-of-sync of these two SOA tracers was more clearly seen in the diurnal variation of their ratio, as seen in Fig. 7a. A daytime dip in DHOPA/phthalic acid was evident in five out of the six day-night cycles. This field observation implies that nighttime processes favored sustaining DHOPA while daytime processes activated the formation of phthalic acids or strong night loss processes of phthalic acid might be in operation. The variation of DHOPA was more in sync with that of pinic acid (Fig. 7b), supporting the suggestion of nighttime chemistry possibly at play. 3-MBTCA/pinic acid ratio is also plotted in a similar way (Fig. 7a), showing a slight increase of 3-MBTCA in comparison to pinic acid in the day time. This may partially be explained by its formation involving $NO_x$ chemistry (to be discussed in section 3.6). We note the small relative increase of 3-MBTCA in daytime had a negligible impact on the correlation between 3-MBTCA and pinic acid, which was positively correlated with a R of 0.82 (Fig. 6c). Such contrasts or similarities were only observable with the hourly tracer measurements. Although crude in quality, these field observations nevertheless provide threads of hint for future chamber experiments in furthering the utility of molecular source markers in atmospheric chemistry studies.

We next examine the varying extent of enhancement of precursor-specific SOA. SOA attributable to the three precursors (α-pinene, toluene, and naphthalene) was estimated by applying the tracer-based method (Al-Naiema et al., 2020; Kleindienst et al., 2007, 2012). In the tracer-based method, the mass fraction of tracer compounds to SOA derived from a hydrocarbon precursor ($f^i_{tracer}$) was determined in chamber studies. The chamber-derived mass fractions are 0.1680 ± 0.0081, 0.00198 ± 0.0016, and 0.0199 ± 0.0084 for the SOA tracers formed from oxidation of α-pinene, toluene, and naphthalene, respectively. SOA mass attributable to a certain VOC precursor was then calculated from the ambient tracer concentration ($C^i_{tracer}$) using the equation below.

$$SOA_i = \frac{C^i_{tracer}}{f^i_{tracer}}$$

The sum of individual group SOA estimated this way is denoted as $\Sigma SOA_{tracers}$ hereafter for the ease of reference.

The time series of SOA mass concentrations derived from the three precursor groups are shown in Fig. 8. The episode-wide averages are compared with the non-episodic average in Fig. S10. During the five episodes, the $\Sigma SOA_{tracers}$ concentrations were elevated by 3–9 times when comparing with the non-episode hours. Notably, the proportion by the SOA from these precursors to the total OA has increased from 15% during the non-episodes to 20–53% during the episodic hours. Among the three groups of SOA, toluene-derived SOA contributed the most throughout the five episodes (78–86%), indicating the importance of toluene as an SOA precursor in Shanghai. Toluene has a wide range of sources (e.g., solvent use in various industries and vehicular emissions) (Liu et al., 2008). The moderate correlation coefficient between toluene and CO (R = 0.64) tends to substantiate a significant contribution from vehicle exhaust.

Among the five episodes, E5 was the longest and had the most severe pollution level. During E5, the average wind speed was merely 1.57 m/s and air masses were circulating locally (Fig. 2). Such stagnant conditions

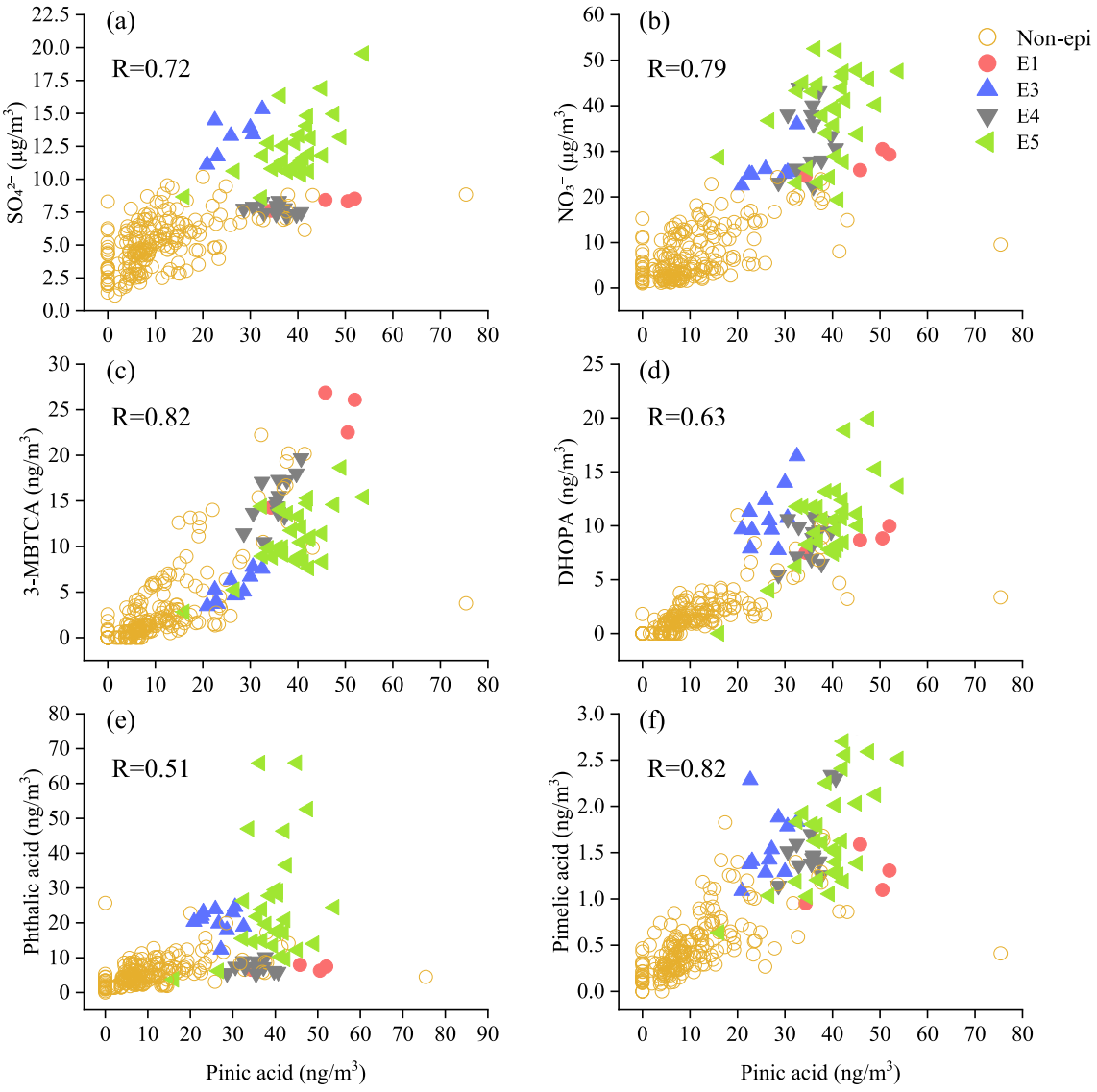


**Fig. 6.** Correlation scatter plots of pinic acid with select known secondary products including sulfate, nitrate, the other three SOA tracers (3-MBTCA, DHOPA, and phthalic acid), and pimelic acid. The Pearson correlation coefficients of the above pairs are all better that between pinic acid and BC (R: 0.45) (not shown).

were conducive to cause accumulation of primary pollutants and subsequently facilitate the formation of secondary pollutants. In E5, the $PM_{2.5}$ level was elevated to an episode-average of 113 μg/m$^3$ while the average $PM_{2.5}$ was 32 μg/m$^3$ during the non-episodes. Among the other major components, $NO_3^-$ sharply increased from 7.2 to 37.9 μg/m$^3$, $NH_4^+$ was elevated from 3.8 to 16.1 μg/m$^3$, and $SO_4^{2-}$ underwent a mild increase (from 5.0 to 12.3 μg/m$^3$). The hourly estimated $SOA_{tol}$ varied from 2.0 to 10.0 μg/m$^3$, accounting for 10.7–32.3% of OA measured by AMS while 1.9–7.7% of $PM_{2.5}$. The hourly estimated $SOA_{Nap}$ varied from 0.2 to 3.3 μg/m$^3$, accounting for 1.5–12.5% of OA measured by AMS and 0.2–3.0% of $PM_{2.5}$.

The time series of $O_x$ (the sum of $O_3$ and $NO_2$) is displayed in Fig. 8d, in parallel with SOA estimate by tracers and SOA estimate by PMF analysis of AMS data (see section 3.5). No notable rise of $O_x$ was observed during the episodic periods except for E5. A previous study found a suppression effect of $PM_{2.5}$ on ozone concentration under high PM polluted conditions (60–100 μg/m$^3$) based on both observation and model simulation data (Li et al., 2019). This suppression effect by excessive PM may partially explain the relative stable $O_x$ concentration especially during the episodic hours, as the $PM_{2.5}$ concentration ranged from 80 to 112 μg/m$^3$ during the five episodes. The MIR values of 0.7–1.6, 1.0–1.9, and 1.0–1.4 were observed for $O_3$, $NO_2$, and $O_x$, respectively. The results suggest that the sharp increase in SOA was mainly driven by the buildup of the emitted precursors and/or the concentration-dependent oxidation chemistry. In E5, the accumulation of SOA was in concurrence with a moderately higher level of $O_x$. The elevated $O_x$ may have played a facilitating role in additional SOA formation during E5.

### 3.5. Comparison of tracer-derived SOA mass and AMS PMF resolved SOA mass

Positive matrix factorization analysis of the AMS sata resolved five OA factors, including two primary OA factors (i.e., hydrocarbon-like OA factor (HOA), cooking-related OA factor) and three secondary OA factors (i.e., two semi-volatile oxygenated OA factors (SVOOA1, SVOOA2) and one low-volatile oxygenated OA factor (LVOOA)). The mass spectra for the PMF-resolved individual OA factors are provided in Fig. S11. The aggregated mass concentration attributed from the three AMS secondary OA factors is referred to as $\Sigma SOA_{AMS}$ in the ensuing text. The detailed AMS data and the OA source analysis using AMS data will be reported in a separate paper. We here only include a brief description of each factor

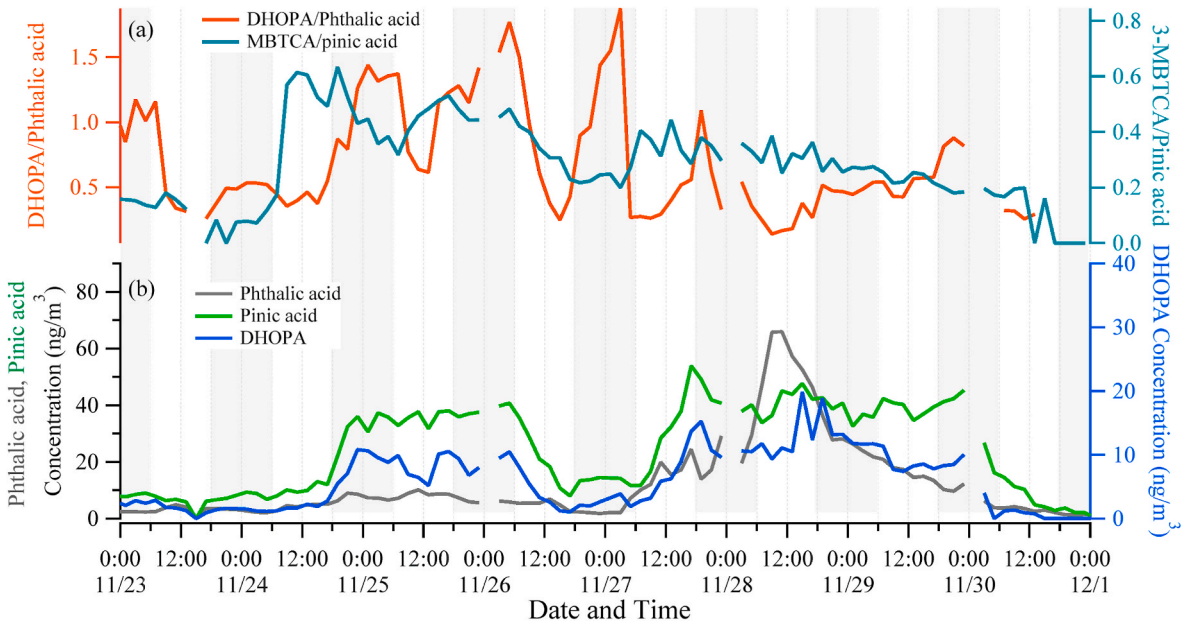


**Fig. 7.** Diurnal variation of (a) the ratio of DHOPA/phthalic acid and the ratio of 3-MBTCA/pinic acid, and (b) the time series of DHOPA, phthalic acid, and pinic acid during E4 and E5 episodes. Nighttime (6 p.m.-6 am) hours are shaded in gray. Note different concentration scales in (b) for the three SOA tracers.

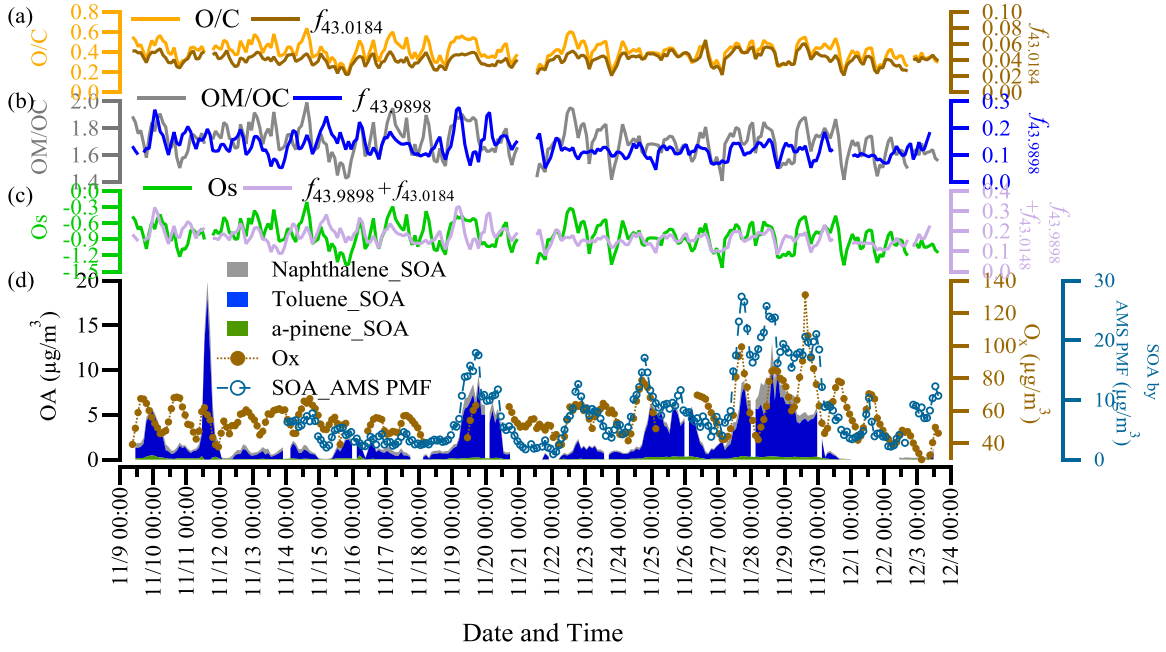


**Fig. 8.** (a) Time series of O/C ratio and $f_{43.0184}$; (b) Time series of OM/OC ratio and $f_{43.8898}$; (c) Time series of oxidation state ($\overline{OSc}$), ($f_{43.0184} + f_{43.8898}$), and $f_{43.0184}/f_{43.8898}$; (d) Time series of the SOA mass concentration derived from each VOC precursor, the aggregated mass concentrations derived from AMS PMF resolved secondary factors, and the concentration of $O_x$. The five episodes are shaded in gray.

and focus on the comparison of the prupose of AMS-derived SOA mass and the tracer-derived SOA mass. The OM/OC ratios of HOA and SVOOA2 are 1.40 and 1.46, and both factors correlate positively with $NO_x$, with a Pearson *r* at 0.81 and 0.67, respectively (Fig. S11). Such characteristics indicate that SVOOA2 is likely a direct oxidation factor of HOA, and the correlation between the two factors ($r = 0.62$) tends to confirm this association. In comparison, the SVOOA1 and LVOOA are more oxygenated, with an OM/OC ratio at 1.87 and 2.01 and an O/C ratio at 0.54 and 0.66, respectively. SVOOA1 has a good correlation with nitrate (r = 0.86) while LVOOA has a good correlation with sulfate (Fig. S11), consistent with the different aging degree of these two oxygenated OA factors.

The time series of $\Sigma SOA_{tracers}$ and $\Sigma SOA_{AMS}$ are compared in Fig. 8d, and the correlation plots of $\Sigma SOA_{tracers}$ vs $SOA_{AMS}$ (both the sum and the dividual SOA factors) are shown in Fig. 9. In general, the total SOA mass derived from the two approaches varied in sync (Fig. 8d) and well correlated (Fig. 9a, R = 0.84). When breaking the $\Sigma SOA_{AMS}$ into the three individual SOA factors, one can see that SVOOA1 and LVOOA drive the correlation while SVOOA2 has a much weakened correlation with $\Sigma SOA_{tracers}$ (Fig. 9b, R = 0.37).

The $\Sigma SOA_{AMS}$ was consistently larger than $\Sigma SOA_{tracers}$, with the slope of 1.77. The average $\Sigma SOA_{tracer}$ was 2.62 μg/m$^3$, in comparison with the

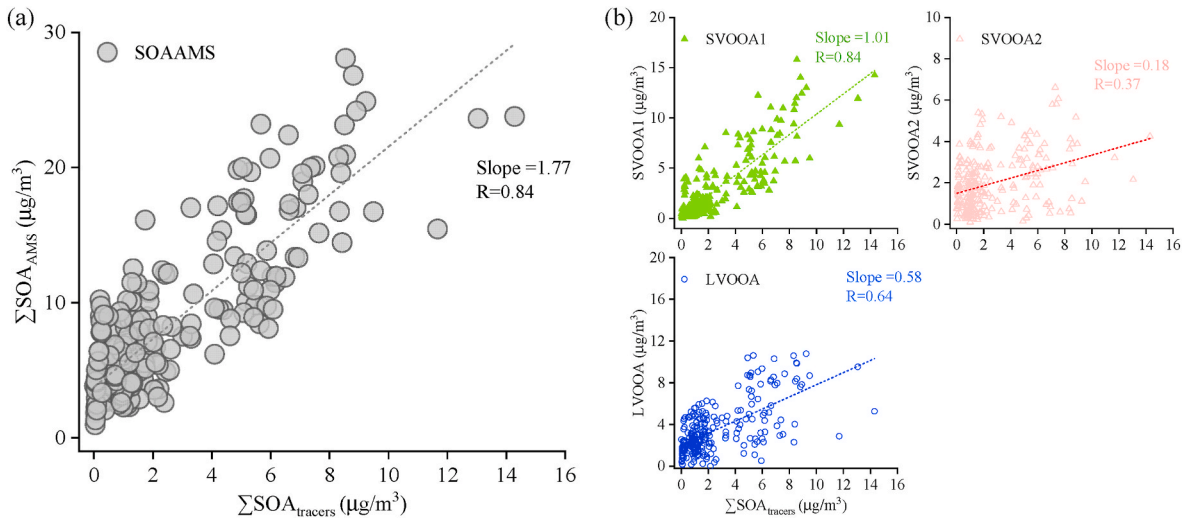


**Fig. 9.** Correlation plots of SOA mass concentrations derived from AMS versus SOA by the tracer-based method. (a) The sum of all SOA factors by AMS data vs. $\Sigma SOA_{tracers}$; (b) Individual SOA factors by AMS (SVOOA1, SVOOA2, and LVOOA) vs. $\Sigma SOA_{tracers}$.

average $\Sigma SOA_{AMS}$ at 7.86 μg/m$^3$. This is expected considering $\Sigma SOA_{tracers}$ only account for three precursor groups. We should bear in mind that the tracer-based method only considers the SOA derived from a limited set of VOC precursors and it uses one single mass fraction derived from laboratory studies to represent a much diverse range of SOA formation conditions inherent to ambient environments. Thus, SOA from other un-tracked precursors is not accounted for in the estimated $\Sigma SOA_{tracers}$. Additionally, the oversimplification in using a uniform mass fraction imparts a significant and yet unquantified uncertainty to the $\Sigma SOA_{tracers}$ quantity. $\Sigma SOA_{tracers}$ by no means gives an accurate representation of the amount of bulk SOA. Nevertheless, the fact that the two approaches varied in sync supports the utility of precursor-specific tracer measurements and that $\Sigma SOA_{tracers}$ estimates are at least semi-quantitatively indicative.

### 3.6. *Evidence for fresh SOA formation in urban Shanghai*

Two α-pinene-derived SOA tracers, pinic acid and 3-MBTCA, were consistently detected during the field campaign. They showed distinctively different diurnal patterns. Pinic acid had no discernible diurnal variation while 3-MBTCA showed a slight increase in the afternoons (Fig. 4). Furthermore, a negative correlation was found between 3-MBTCA and the mass ratio of pinic acid to 3-MBTCA (abbreviated as P/M), as plotted in Fig. 10a, with slopes of −1.34 and −1.03 for episodes and non-episodes, respectively.

Pinic acid is an early generation SOA product of α-pinene oxidation processes while 3-MBTCA is a later generation product, as illustrated in the simplified oxidation mechanism of α-pinene by $O_3$ (Fig. 10b) (Kristensen et al., 2014; Ma et al., 2008; Szmigielski et al., 2007). It has been proposed the ratio of early generation product to the later generation product (i.e., pinic acid/MBTCA) could serve as an indicator of the aging of the α-pinene derived aerosols. An average of 3.6 ± 1.5 was found for the episodes during this campaign, which is much less than the reported average ratio of pinic acid plus pinonic acid to MBTCA (7.19) for the fresh SOA measured at a rural site in the central Pearl River Delta (PRD) region (Ding et al., 2011). This result suggests a less-aged α-pinene derived SOA. The significant correlation between pinic acid and 3-MBTCA (R = 0.82) (Fig. 6c) also supports the suggestion of relatively

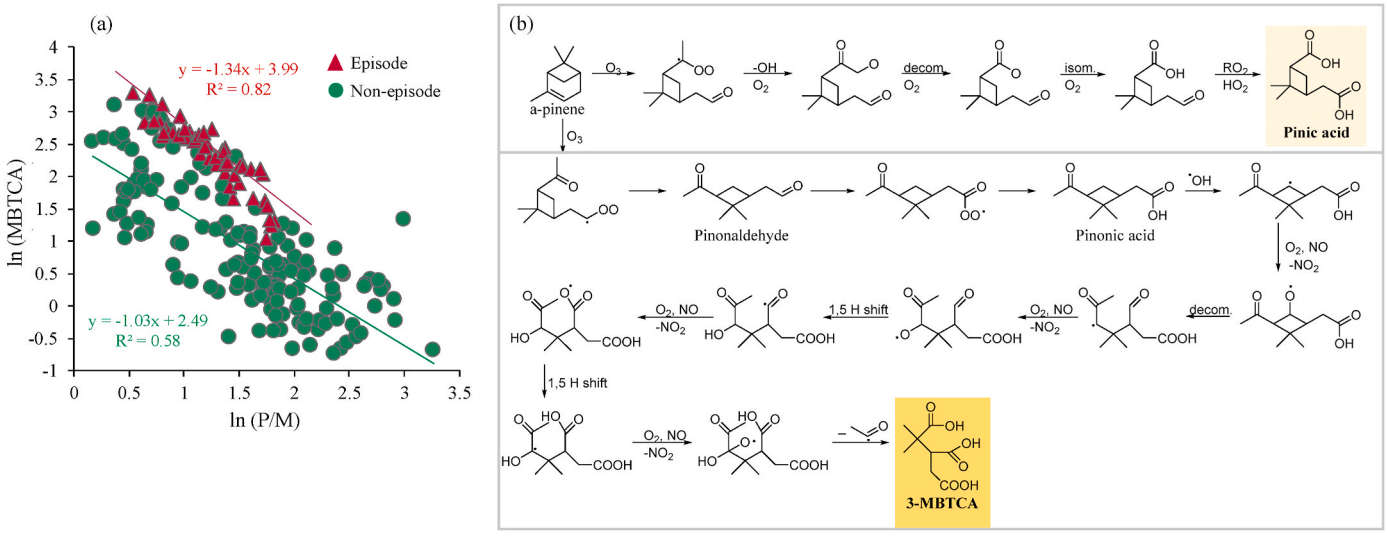


**Fig. 10.** (a) A negative correlation is observed between ln (P/M) and ln (3-MBTCA). P/M is the ratio of pinic acid to 3-methyl-1,2,3-butanetricarboxylic acid (3-MBTCA). Red triangles represent data collected during episodes and green circles represent data during non-episodes. Linear correlations are fitted separately for episodic and non-episodic hours. (b) Simplified mechanism of α-pinene oxidization to pinic acid (early product) and 3-MBTCA (late product). (For interpretation of the references to color in this figure legend, the reader is referred to the Web version of this article.)

**Table 3**
The distribution of diagnostic parameters of $f_{43.0184}$ (ratio of $m/z$ 43.0184 to the total signals in the component mass spectrum), $f_{43.9898}$ (ratio of $m/z$ 43.9898 to the total signals in the component mass spectrum), ($f_{43.0184} + f_{43.8898}$), O/C, OM/OC, and oxidation state ($\overline{OSc}$).

| | $f_{43.8898}$ | $f_{43.0184}$ | $f_{43.8898} + f_{43.0184}$ | O/C | OM/OC | $-\overline{OSc}$ |
|---|---|---|---|---|---|---|
| Non-epi | 0.13 ± 0.07 | 0.04 ± 0.02 | 0.17 ± 0.08 | 0.40 ± 0.20 | 1.69 ± 0.76 | 0.84 ± 0.43 |
| All-epi | 0.13 ± 0.06 | 0.04 ± 0.02 | 0.17 ± 0.07 | 0.41 ± 0.17 | 1.70 ± 0.70 | 0.84 ± 0.36 |
| E1 | 0.20 ± 0.02 | 0.05 ± 0.01 | 0.25 ± 0.03 | 0.49 ± 0.06 | 1.81 ± 0.21 | 0.64 ± 0.08 |
| E2 | 0.16 ± 0.02 | 0.05 ± 0.00 | 0.16 ± 0.01 | 0.42 ± 0.02 | 1.72 ± 0.10 | 0.83 ± 0.05 |
| E3 | 0.14 ± 0.03 | 0.04 ± 0.01 | 0.18 ± 0.04 | 0.42 ± 0.09 | 1.72 ± 0.34 | 0.82 ± 0.17 |
| E4 | 0.11 ± 0.02 | 0.04 ± 0.01 | 0.15 ± 0.03 | 0.37 ± 0.08 | 1.65 ± 0.35 | 0.92 ± 0.20 |
| E5 | 0.12 ± 0.04 | 0.05 ± 0.01 | 0.17 ± 0.05 | 0.42 ± 0.13 | 1.71 ± 0.53 | 0.84 ± 0.27 |

fresh α-pinene SOA. A previous study reported a null correlation for the aged α-pinene SOA formation at a receptor site in the Pearl River Delta, China (Ding et al., 2011).

This finding is consistent with a previous comparison study conducted between Hong Kong and Beijing revealing that the ambient atmosphere in Beijing had higher SOA formation potential than that in Hong Kong after aging in a Potential Aerosol Mass (PAM) reactor (Li et al., 2019a). We may extrapolate that the comparatively fresh secondarily formed OA and stronger potential for SOA formation is likely a typical feature of the urban atmosphere in cities such as Shanghai and Beijing because of bountiful VOC precursors.

Further evidence was also found with the concurrent AMS measurements. $f_{43.0184}$ and $f_{43.8898}$ are the ratio of $m/z$ 43.0184 ($C_2H_3O^+$) and $m/z$ 43.9898 ($CO_2^+$) to the total signals in the component mass spectra, respectively. The fragments of $m/z$ 43.9898 and $m/z$ 43.0184 are reported to be mainly attributed to thermal decarboxylation of organic acids and decomposition of non-acid oxygenates respectively, and they are used to address the evolution of organic aerosols in the atmosphere (Alfarra et al., 2004; Ng et al., 2010). Aging of oxygenated OA can be observed in the form of decreasing of $f_{43.0184}$ $m/z$ and the increasing of $f_{43.8898}$ $m/z$ as well as O/C and OM/OC ratios. The time series of $f_{43.0184}$, $f_{43.8898}$, ($f_{43.0184} + f_{43.8898}$), oxidation state (Os), O/C and OM/OC ratios are plotted in Fig. 8a–c. Comparing episodes with non-episode, no noticeable elevation in the abovementioned parameters were observed during episodes. For example, the O/C ratios during the five episodes were 0.49 ± 0.06, 0.42 ± 0.02, 0.42 ± 0.07, 0.37 ± 0.08, and 0.42 ± 0.13, in comparison with that during the non-episode hours (0.40 ± 0.20). These O/C ratios are closer to the ratio for the SVOOA1 (0.54) than the other OA factors, indicating the more significant contribution by SVOOA1 throughout our measurement period. The distribution of the six diagnostic parameters is summarized in Table 3. This dataset falls exclusively within the range of SVOOA in the triangular space proposed by Ng et al. (2010), in agreement with the conclusion from the SOA tracer data that the SOA formed in urban Shanghai was quite fresh. The comparable values of the seven parameters during episodes and non-episode confirm that the eruption of SOA mass was more closely related to the early generation of SOA products and thus the local emissions of precursors.

## 4. Summary

An online instrument, TAG, for the speciation of individual organic compounds was deployed in a three-week-long field campaign conducted at a monitoring station in urban Shanghai, together with side-by-side online measurements of $PM_{2.5}$ mass concentration and its major components. A group of 30 polar organic compounds, including a subset of SOA tracers, were quantified by TAG. Five episodes were observed during the campaign, with the $PM_{2.5}$ concentration exceeding 100 μg/m$^3$. The formation of SOA compounds was found significantly enhanced during the episodic periods, and the strongest enhancement was the monoaromatics-derived SOA tracer. Through examining the ratio of early to late generation of monoterpene oxidation products and the O/C ratio in bulk OA, we found evidence to indicate that SOA formation in urban Shanghai during this campaign was quite fresh. This is the first time that online speciation of individual organic compounds is achieved, especially those serving as specific source tracers in a polluted environment in China. The finding that secondary formations contribute dominantly to the episode eruption, including both inorganic and organic fractions, provides valuable observation-based data for future policy implementation.

## Credit author statement

Xiao He: Conceptualization, Methodology, Investigation, Formal analysis, Writing – Original Draft. Qiongqiong Wang: Methodology, Validation. X.H. Hilda Huang: Data Curation, Writing – Review & Editing. Dan Dan Huang: Formal analysis, Data Curation. Min Zhou: Validation, Data Curation. Liping Qiao: Validation, Data Curation. Shuhui Zhu: Validation, Data Curation. Ying-ge Ma: Data Curation. Hong-li Wang: Validation, Data Curation. Li Li: Conceptualization, Funding acquisition. Cheng Huang: Conceptualization, Project administration, Funding acquisition. Wen Xu: Data Curation. Douglas R. Worsnop: Formal analysis, Mentorship. Allen H. Goldstein: Formal analysis, Writing – Review & Editing, Mentorship. Jian Zhen Yu: Conceptualization, Methodology, Writing – Review & Editing, Funding acquisition.

## Declaration of competing interest

The authors declare that they have no known competing financial interests or personal relationships that could have appeared to influence the work reported in this paper.

## Acknowledgements

We are grateful for funding support by the National Key R&D Program of China (2018YFC0213800), the National Natural Science Foundation of China (41875161), the Hong Kong Research Grant Council (C5004-15E, 16305418, and R6011-18), and the Special Fund Project for Science and Technology Innovation Strategy of Guangdong Province (2019B121205004).

## Appendix A. Supplementary data

Supplementary data to this article can be found online at https://doi.org/10.1016/j.atmosenv.2020.117807.

## References


Al-Naiema, I.M., Offenberg, J.H., Madler, C.J., Lewandowski, M., Kettler, J., Fang, T., Stone, E.A., 2020. Secondary organic aerosols from aromatic hydrocarbons and their contribution to fine particulate matter in Atlanta, Georgia. Atmos. Environ. 223.

Alfarra, M.R., Coe, H., Allan, J.D., Bower, K.N., Boudries, H., Canagaratna, M.R., Jimenez, J.L., Jayne, J.T., Garforth, A.A., Li, S.M., Worsnop, D.R., 2004. Characterization of urban and rural organic particulate in the lower Fraser valley using two aerodyne aerosol mass spectrometers. Atmos. Environ. 38, 5745–5758.

Bauer, H., Claeys, M., Vermeylen, R., Schueller, E., Weinke, G., Berger, A., Puxbaum, H., 2008. Arabitol and mannitol as tracers for the quantification of airborne fungal spores. Atmos. Environ. 42, 588–593.

Canagaratna, M.R., Jayne, J.T., Jimenez, J.L., Allan, J.D., Alfarra, M.R., Zhang, Q., Onasch, T.B., Drewnick, F., Coe, H., Middlebrook, A., Delia, A., Williams, L.R., Trimborn, A.M., Northway, M.J., DeCarlo, P.F., Kolb, C.E., Davidovits, P., Worsnop, D.R., 2007. Chemical and microphysical characterization of ambient aerosols with the aerodyne aerosol mass spectrometer. Mass Spectrom. Rev. 26, 185–222.

Ding, X.A., Wang, X.M., Zheng, M., 2011. The influence of temperature and aerosol acidity on biogenic secondary organic aerosol tracers: observations at a rural site in the central Pearl River Delta region, South China. Atmos. Environ. 45, 1303–1311.

Fu, P.Q., Kawamura, K., Pavuluri, C.M., Swaminathan, T., Chen, J., 2010. Molecular characterization of urban organic aerosol in tropical India: contributions of primary emissions and secondary photooxidation. Atmos. Chem. Phys. 10, 2663–2689.

Furger, M., Minguillon, M.C., Yadav, V., Slowik, J.G., Huglin, C., Frohlich, R., Petterson, K., Baltensperger, U., Prevot, A.S.H., 2017. Elemental composition of ambient aerosols measured with high temporal resolution using an online XRF spectrometer. Atmos. Meas. Tech. 10.

Guo, S., Hu, M., Guo, Q.F., Zhang, X., Zheng, M., Zheng, J., Chang, C.C., Schauer, J.J., Zhang, R.Y., 2012. Primary sources and secondary formation of organic aerosols in Beijing, China. Environ. Sci. Technol. 46, 9846–9853.

He, X., Huang, X.H.H., Chow, K.S., Wang, Q.Q., Zhang, T., Wu, D., Yu, J.Z., 2018. Abundance and sources of phthalic acids, benzene-tricarboxylic acids, and phenolic acids in PM2.5 at urban and suburban sites in southern China. Acs. Earth Space Chem. 2, 147–158.

Ho, K.F., Engling, G., Ho, S.S.H., Huang, R.J., Lai, S.C., Cao, J.J., Lee, S.C., 2014. Seasonal variations of anhydrosugars in PM2.5 in the Pearl River Delta region, China. Tellus B 66.

Ho, K.F., Ho, S.S.H., Huang, R.J., Chuang, H.C., Cao, J.J., Han, Y.M., Lui, K.H., Ning, Z., Chuang, K.J., Cheng, T.J., Lee, S.C., Hu, D., Wang, B., Zhang, R.J., 2016. Chemical composition and bioreactivity of PM2.5 during 2013 haze events in China. Atmos. Environ. 126, 162–170.

Hu, D., Bian, Q., Li, T.W.Y., Lau, A.K.H., Yu, J.Z., 2008. Contributions of isoprene, monoterpenes, beta-caryophyllene, and toluene to secondary organic aerosols in Hong Kong during the summer of 2006. J. Geophys. Res. Atmos. 113.

Huttunen, K., Siponen, T., Salonen, I., Yli-Tuomi, T., Aurela, M., Dufva, H., Hillamo, R., Linkola, E., Pekkanen, J., Pennanen, A., Peters, A., Salonen, R.O., Schneider, A., Tiittanen, P., Hirvonen, M.R., Lanki, T., 2012. Low-level exposure to ambient particulate matter is associated with systemic inflammation in ischemic heart disease patients. Environ. Res. 116, 44–51.

Hyder, M., Genberg, J., Sandahl, M., Swietlicki, E., Jonsson, J.A., 2012. Yearly trend of dicarboxylic acids in organic aerosols from south of Sweden and source attribution. Atmos. Environ. 57, 197–204.

Isaacman, G., Kreisberg, N.M., Yee, L.D., Worton, D.R., Chan, A.W.H., Moss, J.A., Hering, S.V., Goldstein, A.H., 2014. Online derivatization for hourly measurements of gas- and particle-phase semi-volatile oxygenated organic compounds by thermal desorption aerosol gas chromatography (SV-TAG). Atmos. Meas. Tech. 7, 4417–4429.

Jayne, J.T., Leard, D.C., Zhang, X.F., Davidovits, P., Smith, K.A., Kolb, C.E., Worsnop, D. R., 2000. Development of an aerosol mass spectrometer for size and composition analysis of submicron particles. Aerosol Sci. Technol. 33, 49–70.

Jimenez, J.L., Jayne, J.T., Shi, Q., Kolb, C.E., Worsnop, D.R., Yourshaw, I., Seinfeld, J.H., Flagan, R.C., Zhang, X.F., Smith, K.A., Morris, J.W., Davidovits, P., 2003. Ambient aerosol sampling using the aerodyne aerosol mass spectrometer. J. Geophys. Res. Atmos. 108.

Kim, N., Park, M., Yum, S.S., Park, J.S., Song, I.H., Shin, H.J., Ahn, J.Y., Kwak, K.H., Kim, H., Bae, G.N., Lee, G., 2017. Hygroscopic properties of urban aerosols and their cloud condensation nuclei activities measured in Seoul during the MAPS Seoul campaign. Atmos. Environ. 153, 217–232.

Kleindienst, T.E., Jaoui, M., Lewandowski, M., Offenberg, J.H., Docherty, K.S., 2012. The formation of SOA and chemical tracer compounds from the photooxidation of naphthalene and its methyl analogs in the presence and absence of nitrogen oxides. Atmos. Chem. Phys. 12, 8711–8726.

Kleindienst, T.E., Jaoui, M., Lewandowski, M., Offenberg, J.H., Lewis, C.W., Bhave, P.V., Edney, E.O., 2007. Estimates of the contributions of biogenic and anthropogenic hydrocarbons to secondary organic aerosol at a southeastern US location. Atmos. Environ. 41, 8288–8300.

Kristensen, K., Cui, T., Zhang, H., Gold, A., Glasius, M., Surratt, J.D., 2014. Dimers in alpha-pinene secondary organic aerosol: effect of hydroxyl radical, ozone, relative humidity and aerosol acidity. Atmos. Chem. Phys. 14, 4201–4218.

Lelieveld, J., Barlas, C., Giannadaki, D., Pozzer, A., 2013. Model calculated global, regional and megacity premature mortality due to air pollution. Atmos. Chem. Phys. 13, 7023–7037.

Li, K., Jacob, D.J., Liao, H., Zhu, J., Shah, V., Shen, L., Bates, K.H., Zhang, Q., Zhai, S.X., 2019. A two-pollutant strategy for improving ozone and particulate air quality in China. Nat. Geosci. 12, 906-910.

Li, J.J., Liu, Q.Y., Li, Y.J., Liu, T.Y., Huang, D.D., Zheng, J., Zhu, W.F., Hu, M., Wu, Y.S., Lou, S.R., Hallquist, A.M., Hallquist, M., Chan, C.K., Canonaco, F., Prevot, A.S.H., Fung, J.C.H., Lau, A.K.H., Yu, J.Z., 2019a. Characterization of aerosol aging potentials at suburban sites in northern and southern China utilizing a potential aerosol mass (Go:PAM) reactor and an aerosol mass spectrometer. J. Geophys. Res. Atmos. 124, 5629–5649.

Li, R., Wang, Q., He, X., Zhu, S., Zhang, K., Duan, Y., Fu, Q., Qiao, L., Wang, Y., Huang, L., Li, L., Yu, J.Z., 2020. Source apportionment of PM2.5 in Shanghai based on hourly molecular organic markers and other source tracers. Atmos. Chem. Phys. Discuss.

Li, X.D., Yang, Z., Fu, P.Q., Yu, J., Lang, Y.C., Liu, D., Ono, K., Kawamura, K., 2015. High abundances of dicarboxylic acids, oxocarboxylic acids, and alpha-dicarbonyls in fine aerosols (PM2.5) in Chengdu, China during wintertime haze pollution. Environ. Sci. Pollut. Res. 22, 12902–12918.

Li, Y.J., Sun, Y., Zhang, Q., Li, X., Li, M., Zhou, Z., Chan, C.K., 2017. Real-time chemical characterization of atmospheric particulate matter in China: a review. Atmos. Environ. 158, 270–304.

Liu, Y., Shao, M., Fu, L.L., Lu, S.H., Zeng, L.M., Tang, D.G., 2008. Source profiles of volatile organic compounds (VOCs) measured in China: Part I. Atmos. Environ. 42, 6247–6260.

Ma, Y., Russell, A.T., Marston, G., 2008. Mechanisms for the formation of secondary organic aerosol components from the gas-phase ozonolysis of alpha-pinene. Phys. Chem. Chem. Phys. 10, 4294–4312.

Mochida, M., Kawabata, A., Kawamura, K., Hatsushika, H., Yamazaki, K., 2003. Seasonal variation and origins of dicarboxylic acids in the marine atmosphere over the western North Pacific. J. Geophys. Res. Atmos. 108.

Narukawa, M., Kawamura, K., Anlauf, K.G., Barrie, L.A., 2003. Fine and coarse modes of dicarboxylic acids in the Arctic aerosols collected during the Polar Sunrise Experiment 1997. J. Geophys. Res. Atmos. 108.

Ng, N.L., Canagaratna, M.R., Zhang, Q., Jimenez, J.L., Tian, J., Ulbrich, I.M., Kroll, J.H., Docherty, K.S., Chhabra, P.S., Bahreini, R., Murphy, S.M., Seinfeld, J.H., Hildebrandt, L., Donahue, N.M., DeCarlo, P.F., Lanz, V.A., Prevot, A.S.H., Dinar, E., Rudich, Y., Worsnop, D.R., 2010. Organic aerosol components observed in northern Hemispheric datasets from Aerosol Mass Spectrometry. Atmos. Chem. Phys. 10, 4625–4641.

Petit, J.E., Favez, O., Albinet, A., Canonaco, F., 2017. A user-friendly tool for comprehensive evaluation of the geographical origins of atmospheric pollution: wind and trajectory analyses. Environ. Model. Software 88, 183–187.

Pope, C.A., Bhatnagar, A., McCracken, J.P., Abplanalp, W., Conklin, D.J., O'Toole, T., 2016. Exposure to fine particulate air pollution is associated with endothelial injury and systemic inflammation. Circ. Res. 119, 1204-+.

Qiao, L.P., Cai, J., Wang, H.L., Wang, W.B., Zhou, M., Lou, S.R., Chen, R.J., Dai, H.X., Chen, C.H., Kan, H.D., 2014. PM2.5 constituents and hospital emergency-room visits in Shanghai, China. Environ. Sci. Technol. 48, 10406–10414.

Rastogi, N., Patel, A., Singh, A., Singh, D., 2015. Diurnal variability in secondary organic aerosol formation over the Indo-Gangetic Plain during winter using online measurement of water-soluble organic carbon. Aerosol. Air Qual. Res. 15, 2225–2231.

Saarikoski, S., Timonen, H., Saarnio, K., Aurela, M., Jarvi, L., Keronen, P., Kerminen, V. M., Hillamo, R., 2008. Sources of organic carbon in fine particulate matter in northern European urban air. Atmos. Chem. Phys. 8, 6281–6295.

Simoneit, B.R.T., Medeiros, P.M., Didyk, B.M., 2005. Combustion products of plastics as indicators for refuse burning in the atmosphere. Environ. Sci. Technol. 39, 6961–6970.

Spira-Cohen, A., Chen, L.C., Kendall, M., Sheesley, R., Thurston, G.D., 2010. Personal exposures to traffic-related particle pollution among children with asthma in the South Bronx, NY. J. Expo. Sci. Environ. Epidemiol. 20, 446–456.

Stein, A.F., Draxler, R.R., Rolph, G.D., Stunder, B.J.B., Cohen, M.D., Ngan, F., 2015. Noaa's hysplit atmospheric transport and dispersion modeling system. Bull. Am. Meteorol. Soc. 96, 2059–2077.

Stone, E.A., Zhou, J.B., Snyder, D.C., Rutter, A.P., Mieritz, M., Schauer, J.J., 2009. A comparison of summertime secondary organic aerosol source contributions at contrasting urban locations. Environ. Sci. Technol. 43, 3448–3454.

Szmigielski, R., Surratt, J.D., Gomez-Gonzalez, Y., Van der Veken, P., Kourtchev, I., Vermeylen, R., Blockhuys, F., Jaoui, M., Kleindienst, T.E., Lewandowski, M., Offenberg, J.H., Edney, E.O., Seinfeld, J.H., Maenhaut, W., Claeys, M., 2007. 3-methyl-1,2,3-butanetricarboxylic acid: an atmospheric tracer for terpene secondary organic aerosol. Geophys. Res. Lett. 34.

Wang, Q.Q., He, X., Zhou, M., Huang, D.D., Qiao, L.P., Zhu, S.H., Ma, Y.G., Wang, H.L., Li, L., Huang, C., Huang, X.H.H., Xu, W., Worsnop, D.R., Goldstein, A.H., Yu, J.Z., 2020. Hourly measurements of organic molecular markers in urban Shanghai, China: Primary organic aerosol source identification and observation of cooking aerosol aging. ACS J. Earth Space. Submitted for publication.

Wang, H.Q., Ma, J.M., Shen, Y.J., Wang, Y.A., 2015. Assessment of Ozone Variations and meteorological influences at a rural site in northern Xinjiang. Bull. Environ. Contam. Toxicol. 94, 240–246.

Wang, Q.Q., He, X., Huang, X.H.H., Griffith, S.M., Feng, Y.M., Zhang, T., Zhang, Q.Y., Wu, D., Yu, J.Z., 2017. Impact of secondary organic aerosol tracers on tracer-based source apportionment of organic carbon and PM2.5: a case study in the Pearl River Delta, China. Acs. Earth Space Chem. 1, 562–571.

Wang, Q.Q., Qiao, L.P., Zhou, M., Zhu, S.H., Griffith, S., Li, L., Yu, J.Z., 2018. Source apportionment of PM2.5 using hourly measurements of elemental tracers and major constituents in an urban environment: investigation of time-resolution influence. J. Geophys. Res. Atmos. 123, 5284–5300.

Williams, B.J., Goldstein, A.H., Kreisberg, N.M., Hering, S.V., 2006. An in-situ instrument for speciated organic composition of atmospheric aerosols: thermal Desorption Aerosol GC/MS-FID (TAG). Aerosol Sci. Technol. 40, 627–638.
Zhang, Y.L., Ren, H., Sun, Y.L., Cao, F., Chang, Y.H., Liu, S.D., Lee, X.H., Agrios, K., Kawamura, K., Liu, D., Ren, L.J., Du, W., Wang, Z.F., Prevot, A.S.H., Szida, S., Fu, P. Q., 2017. High contribution of nonfossil sources to submicrometer organic aerosols in Beijing, China. Environ. Sci. Technol. 51, 7842–7852.
Zhao, X.Y., Wang, X.M., Ding, X., He, Q.F., Zhang, Z., Liu, T.Y., Fu, X.X., Gao, B., Wang, Y.P., Zhang, Y.L., Deng, X.J., Wu, D., 2014. Compositions and sources of organic acids in fine particles (PM2.5) over the Pearl River Delta region, south China. J. Environ. Sci. China 26, 110–121.
Zhao, Y.L., Kreisberg, N.M., Worton, D.R., Teng, A.P., Hering, S.V., Goldstein, A.H., 2013. Development of an in situ thermal desorption gas chromatography instrument for quantifying atmospheric semi-volatile organic compounds. Aerosol Sci. Technol. 47, 258–266.